

Strong Spin Hall Effect in the Antiferromagnet PtMn

Yongxi Ou¹, Shengjie Shi¹, D. C. Ralph^{1,2}, and R. A. Buhrman^{1,*}

¹Cornell University, Ithaca, New York 14853, USA

²Kavli Institute at Cornell, Ithaca, New York 14853, USA

Abstract

Effectively manipulating magnetism in ferromagnet (FM) thin film nanostructures with an in-plane current has become feasible since the determination of a “giant” spin Hall effect (SHE) in certain heavy metal (HM)/FM system. Recently, both theoretical and experimental reports indicate that the non-collinear and collinear metallic antiferromagnet (AF) materials can have both a large anomalous Hall effect (AHE) and a strong SHE. Here we report a systematic study of the SHE in PtMn with several PtMn/FM systems. By using interface engineering to reduce the “spin memory loss” we obtain, in the best instance, a spin torque efficiency

$\xi_{DL}^{\text{PtMn}} \equiv T_{\text{int}} \theta_{SH}^{\text{PtMn}} \approx 0.24$, where T_{int} is the effective interface spin transparency. This is more than

twice the previously reported spin torque efficiency for PtMn. We also find that the apparent spin diffusion length in PtMn is surprisingly long, $\lambda_{\xi}^{\text{PtMn}} \approx 2.3\text{nm}$.

SHE in different heavy metal (HM)/ferromagnet (FM) systems¹⁻⁴ can be characterized by the spin Hall ratio (angle) $\theta_{SH} \equiv (2e/\hbar)J_s/J_e$ where J_s is the transverse spin current density generated in the HM and J_e is the applied longitudinal electrical current density. Recently a new class of heavy metal (HM) alloys, the non-collinear antiferromagnet (AF), Mn_3Ir ⁵⁻⁷ and Cu-Au-I type AF, $X_{50}Mn_{50}$ (X=Fe, Pd, Ir, and Pt)⁸⁻¹¹ have been reported to exhibit SHE as spin current sources, with an internal $\theta_{SH}^{PtMn} \approx 0.125$ for PtMn¹⁰, opening up a new area in the rapidly advancing field of “antiferromagnet spintronics”¹²⁻¹⁷. To date research on the SHE from AFs has utilized the implicit assumption that there is no interfacial spin flip scattering or “spin memory loss” (SML)¹⁸ when the spin current traverses the interface to apply a torque to the FM. However the existence of a large SML at some Pt/FM interfaces, together with the negative enthalpy of formation of Mn with both Fe and Ni¹⁹ that can promote interface intermixing, raises the question whether there may also be a significant SML at PtMn/FM interfaces, which would mean that the internal q_{SH}^{PtMn} within PtMn could actually be much higher than previously reported.

We performed a systematic study of the SHE in several PtMn/FM systems employing spin-torque ferromagnetic resonance (ST-FMR)²⁰ on in-plane magnetized (IPM) FM layers and the harmonic response technique (HR)^{21,22} on FM layers with perpendicular magnetic anisotropy (PMA). We also studied samples where a thin (0.25 nm – 0.8 nm) Hf layer is inserted between the PtMn and the FM to suppress strong SML at the interface²³. We find ξ_{DL} to vary significantly with both the deposition order for a given PtMn/FM system and between the different FM systems, but to be relatively consistent between IPM and PMA samples with the same constituents. We also obtained robust current-induced switching in these PMA samples demonstrating the potential for utilizing PtMn in perpendicular magnetic tunneling junction (p-MTJ) and three-terminal device applications.

We first fabricated a series of IPM PtMn/Co bilayer samples by sputter deposition (see Methods) for ST-FMR measurement of the *anti-damping* and *field-like* spin torque efficiencies, ξ_{DL} and ξ_{FL} . The magnetic properties of the samples were also characterized by vibrating sample magnetometry (VSM). Because the order in which the HM and FM layers are deposited affected ξ_{DL} in a previous Pt/Co study²⁴, we grew the PtMn/Co multilayers in both the “standard order” (SO) Ta(1.5)/PtMn(8)/Co(t_{Co})/MgO(1.6)/Ta(1.5) (series A) and in the “reversed order” (RO) MgO(1.6)/Co(t_{Co})/PtMn(8)/MgO(1.6)/Ta(1.5) (series B) (number in parenthesis is thickness in nm). The ST-FMR measurement schematic is illustrated in Fig. 1a. In this technique we obtain the FMR spin torque efficiency ξ_{FMR} that is obtained from the ratio of the symmetric and antisymmetric components of anisotropic magnetoresistance response at the ferromagnetic resonance. The symmetric part is proportional to the *anti-damping* torque and the antisymmetric part is due to the sum of the Oersted field torque and the *field-like* torque (Ref.[24] and Supplementary Information). Fig. 1b shows the results ξ_{FMR} as a function of Co thickness t_{Co} for both the standard (main) and reversed (inset) order samples. For the SO PtMn/Co samples, the spin current in the PtMn layer generates a significant *field-like* torque in addition to the *anti-damping* torque and consequently ξ_{FMR} varies significantly with thickness. By plotting $1/\xi_{FMR}$ vs. $1/t_{Co}$, ξ_{DL} can be determined from the $1/t_{Co} = 0$ intercept and the *field-like* spin torque efficiency ξ_{FL} can be determined from the slope of the plot, provided ξ_{FL} is effectively independent of t_{Co} (Supplementary Information). For the reversed order Co/PtMn samples $\xi_{FMR} (\approx \xi_{DL})$ is essentially constant vs. t_{Co} , indicating ξ_{FL} is negligible (Fig. 1a inset). From this we obtain $\xi_{DL} = 0.16 \pm 0.01$ and $\xi_{FL} = -0.040 \pm 0.008$ for the SO samples and $\xi_{DL} (\text{average}) = 0.19 \pm 0.02$

and $\xi_{FL} \sim 0$ for the RO samples (The minus sign for ξ_{FL} indicates that the *field-like* effective field is *opposite* to the Oersted field).

To further confirm this result with another FM material and to examine the PtMn SHE in structures with PMA, which we were not able to obtain with PtMn/Co bilayers, we replaced Co with Fe₆₀Co₂₀B₂₀ (FeCoB) for the FM layer. First we fabricated two IPM series of PtMn/FeCoB bilayers samples, a SO series (C): Ta(1.5)/PtMn(8)/FeCoB(t_{FeCoB})/MgO(1.6)/Ta(1.5) and a RO series (D): MgO/FeCoB(t_{FeCoB})/PtMn(8)/MgO(1.6)/Ta(1.5). In Fig. 1c we show $1/\xi_{FMR}$ vs.

$1/t_{\text{FeCoB}}^{\text{eff}}$ as obtained for these two sets of samples. From the linear fits to the plots we obtained

$$\xi_{DL} = 0.096 \pm 0.003, \quad \xi_{FL} = -0.043 \pm 0.003 \quad \text{for the SO series (C) samples and}$$

$$\xi_{DL} = 0.174 \pm 0.004, \quad \xi_{FL} = -0.036 \pm 0.002 \quad \text{for the RO series (D) samples.}$$

We also fabricated a SO series (E) of Ta(1.5)/PtMn(8)/FeCoB(t_{FeCoB})/MgO(1.6)/Ta(1.5) with a thinner FM range of $0.4\text{nm} < t_{\text{FeCoB}} < 1.5\text{nm}$, the mid-range of which exhibited PMA without any high temperature annealing (Supplementary Information). The highest out-of-plane anisotropy field $H_{\text{an}} \approx 1.8\text{kOe}$ was achieved with $t_{\text{FeCoB}} \approx 0.8\text{nm}$, which allows us to perform HR measurement of the efficiency of the spin torques exerted on the perpendicularly magnetized FM. The results were $\xi_{DL} = 0.11 \pm 0.02$ and $\xi_{FL} = -0.04 \pm 0.02$, in accord with the ST-FMR values obtained via ST-FMR from the IPM series (C) samples with the same layer structure but thicker

Recent work^{23,25} has shown that the insertion of a thin layer of Hf between FeCoB and the HM in a spin Hall device structure can substantially enhance the PMA, while the thin Hf ($\leq 0.5\text{ nm}$) does not strongly attenuate the spin current. This can be understood as the HM/Hf(~ 0.5)/FeCoB structure having a comparable or smaller SML than that of the seemingly simpler HM/FeCoB

bilayer. Since our SO PtMn/FeCoB structures appear to have a quite significant SML, we fabricated a Ta(1.5)/PtMn(8)/Hf(0.25)/FeCoB(0.8)/ MgO(1.6)/Ta(1.5) sample (F) to determine if an ultra-thin Hf insertion layer could be efficacious in this system for enhancing spin transmission and thus ξ_{DL} . This sample also exhibits PMA without any high-temperature annealing, and using the HR method we measured an exceptionally high damping-like spin torque efficiency $\xi_{DL} = 0.24 \pm 0.03$. Considering that because of the spin back flow effect, not all of the spin current generated within the PtMn will act on the FM^{24,26}, this result indicates that the internal spin Hall ratio is $\theta_{SH}^{PtMn} > 0.24$. We summarize the anti-damping torques for series (A)-(F) in Table I.

To determine the spin diffusion length λ_s^{PtMn} of our PtMn films we then fabricated a set of samples, series (G), with the multilayer stack being Ta(1)/PtMn(t_{PtMn})/Hf(0.8)/FeCoB(0.7)/MgO, where t_{PtMn} ranged from 2 to 8 nm. The thicker Hf spacer promotes strong PMA, with an anisotropy field $H_{an} \approx 1$ Tesla over the full range of PtMn thicknesses studied without annealing. In Fig. 2a we show the results of the HR measurements of *anti-damping* like effective field per unit applied electric field $\Delta H_{DL} / E$ as a function of t_{PtMn} . It can be shown that (see Supplementary Material):

$$\frac{\Delta H_{DL}}{E} = \frac{\sigma_{SH}}{4\pi M_s t_{FM}^{eff}} \frac{G_A}{G_{PtMn} \tanh(t_{PtMn} / \lambda_s^{PtMn}) + G_B} (1 - \text{sech}(t_{PtMn} / \lambda_s^{PtMn})) \quad (1)$$

where $4\pi M_s$ is the magnetization, t_{FM}^{eff} is the effective thickness of the FM layer excluding the dead layer and d_{PtMn} is the thickness of the PtMn, σ_{SH} is the spin Hall conductivity of PtMn

($\sigma_{SH} = \sigma_{PtMn} \theta_{SH}^{PtMn} \hbar / (2e)$), $G_{PtMn} \equiv \sigma_{PtMn} / \lambda_s^{PtMn}$ is the spin conductance of PtMn and G_A and G_B

are parameters depending on the Hf spacer and spin mixing conductance at the Hf/FeCoB interface.

Figure 2a shows a fit of equation (1) to the series (G) results, which gives a spin diffusion length of PtMn $\lambda_{\text{PtMn}} = 2.1\text{nm}$. Our result is much larger than the value 0.5 nm previously reported⁸ from inverse spin Hall effect (ISHE) measurements on NiFe/PtMn. We note that a significant SML layer in the bilayer system due, for example, to reaction of a component of the FM with Mn at PtMn/FM interface can affect the estimation of λ_s^{PtMn} ¹⁸. We also note that Eqn. (1) assumes a constant spin diffusion length that is independent of t_{PtMn} . This is not necessarily the case if the PtMn resistivity ρ_{PtMn} varies with film thickness over the range that we are employing and the Elliot-Yafet spin scattering mechanism dominates, where $\lambda_s^{\text{PtMn}} \propto 1/\rho_{\text{PtMn}}$. Fig. 2b shows the measured resistivity of the PtMn thin layers as a function of t_{PtMn} , which is clearly not a constant. Considered this effect, we can use a “rescaling” method introduced in Ref.[27] to fit our data in Fig. 2a, which yields $\lambda_s^{\text{PtMn}} = 2.3\text{nm}$ for the bulk spin diffusion length (see Supplementary Information). This analysis yields a spin conductance for PtMn $G_{\text{PtMn}} = 1/(\lambda_s^{\text{PtMn}}\rho_{\text{PtMn}}) = 0.37 \times 10^{15} \Omega^{-1}\text{m}^{-2}$, considerably lower than that reported²⁷ for Pt, $G_{\text{Pt}} = 1.3 \times 10^{15} \Omega^{-1}\text{m}^{-2}$ (see also references cited in Ref.[27]). This low PtMn spin conductance could be advantageous in reducing the spin back-flow at an ideal (no SML) PtMn/FM interface (see Ref. [24] and references cited therein).

To demonstrate that PtMn can be used as the source of spin-transfer torque for high-efficiency magnetic switching, we performed current-induced switching using a PtMn(4)/Hf(0.8)/FeCoB(0.7)/MgO sample (H) that as-deposited had strong PMA, and that

exhibited sharp and abrupt magnetic switching under an out of plane field as shown in Fig. 3a. An in-plane field $H_x \geq 50\text{Oe}$ and collinear to the current flow was required to deterministically switch the magnetization, which indicates the existence a weak Dzyaloshinskii-Moriya interaction (DMI) at the Hf/FeCoB interface and a reversal process that proceeds by domain nucleation followed by spin-torque-driven domain expansion²⁸. A typical current switching loop is shown in Fig. 3b, as obtained with $H_y = 200\text{ Oe}$. Fig. 3c shows the spin-torque current switching phase diagram of the same sample. Of course the Hf insertion layer removes the possibility of exchange coupling between the PtMn and the FeCoB, which could add an additional and possibly useful aspect to the simple spin torque switching behavior reported here. We will discuss the switching behavior of PtMn/FM structures with PMA elsewhere.

The value $\xi_{DL} = 0.096 \pm 0.03$ that we obtained from our in-plane magnetized SO PtMn/FeCoB samples is quite similar to that previously reported from inverse spin Hall effect and ST-FMR measurements on in-plane magnetized PtMn/Ni₈₀Fe₂₀ bilayers ($\theta_{SH}^{\text{PtMn}} \approx 0.086$).^{8,10} Also the value for ξ_{FL} that we obtain for this set of PtMn/FeCoB samples is comparable to that reported in Ref.[10] from the shift of the resonance field due to a DC current applied during the FMR measurement of the PtMn/Ni₈₀Fe₂₀ system. In strong contrast to that result, both in our RO PtMn/FeCoB samples and in both versions (SO and RO) of the PtMn/Co sample series ξ_{DL} is much higher. This strongly suggests that a significant SML forms when either FeCoB or Ni₈₀Fe₂₀ is sputter deposited onto PtMn, but that a weaker SML is the result when Co is deposited onto PtMn. For both Co and FeCoB we find that the weakest SML effect occurs when the deposition order is reversed, *i.e.* in the RO samples. We take this as indicating different degrees of undesirable intermixing in the two deposition orders. For the PMA

PtMn/FeCoB/MgO samples that were deposited in the standard order, ξ_{FL} is quite similar to that measured for the SO samples in the case where the FeCoB layers are thicker and hence magnetized in-plane. However by introducing an ultrathin Hf layer between the PtMn and FeCoB layers, which also enhances the PMA, the SML is greatly suppressed and we obtain $\xi_{DL} = 0.24 \pm 0.03$. This sets only a lower bound on the internal spin Hall ratio of the PtMn θ_{SH}^{PtMn} . Since it is reasonable to expect some remnant SML and/or spin backflow effect at this hybrid interface, it is straightforward to speculate that further efforts to engineer the PtMn/FM interface could result in even higher values of the PtMn spin torque efficiency.

The spin diffusion length of PtMn determined in our measurement is also longer than the previously reported value ($<1\text{nm}$)⁸. We tentatively attribute this to the previous study being sensitive to the formation of a SML layer as the PtMn thickness is increased in those PtMn/Ni₈₀Fe₂₀ bilayers, as has recently been discussed for the Pt/Co case^{18,29}. Of course it has to be considered that the PtMn thickness dependence of ξ_{DL} that we observe is due to some thickness dependent change in the electronic properties of the PtMn film rather than a thicker spin diffusion length than previously determined. It is well known that a fairly thick PtMn layer is required to produce the stable antiferromagnetic domains required for exchange biasing of an adjacent FM film. It is not clear however how this AFM stability would act to enhance the spin current that is generated by the electrical current passing the Pt ions, though we notice that there are seemingly contradicted results on the contribution of macroscopic exchange-bias on SHE in IrMn systems^{6,11}. In regard to possible structural changes as a function of PtMn thickness our X-ray diffraction studies (Supplementary Information) do not show any obvious crystalline structure changes for the different thicknesses of PtMn used in this study.

We can use the result for the PtMn spin conductance determined here to further examine the nature of the PtMn/FM interfaces we have studied. In the spin pumping theory^{30,31} of a well-ordered HM/FM interface there is an enhancement of the magnetic damping that varies as $\Delta\alpha = (\gamma\hbar^2 / 8\pi^2 e^2 M_s t_{FM}^{\text{eff}}) G_{\text{eff}}^{\uparrow\downarrow}$ where the effective spin mixing conductance $G_{\text{eff}}^{\uparrow\downarrow} \equiv G^{\uparrow\downarrow} / (1 + 2G^{\uparrow\downarrow} / G_{\text{HM}})$, and $G^{\uparrow\downarrow}$ is the spin mixing conductance of the interface, assuming $\text{Re}G^{\uparrow\downarrow} \gg \text{Im}G^{\uparrow\downarrow}$ (see Supplementary Information). In all four IPM PtMn/FM series studied, the measurement of $\Delta\alpha(t_{FM}^{-1})$ yielded $G_{\text{eff}}^{\uparrow\downarrow} > 0.7 \times 10^{15} \Omega^{-1} \text{m}^{-2}$ (Supplementary Information). With $G_{\text{PtMn}} = 0.37 \times 10^{15} \Omega^{-1} \text{m}^{-2}$, this results in an unphysical (negative) value for $G^{\uparrow\downarrow}$, which means that there must be a significant SML at the PtMn/FM interface and/or a non-ideal damping enhancement at the other FM interface²⁴, neither of which are taken into account in the standard spin pumping theory. (We note that even if we use the previously reported results for PtMn⁸ $\rho_{\text{PtMn}} = 164 \mu\Omega \cdot \text{cm}$ and $\lambda_s^{\text{PtMn}} = 0.5 \text{nm}$ to determine the PtMn spin conductance the $\Delta\alpha(t_{FM}^{-1})$ measurements still yield a negative result for $G^{\uparrow\downarrow}$.)

In summary, depending on the protocol for forming the PtMn/FM interface we have obtained very high *anti-damping* spin torque efficiencies ξ_{DL} from the spin Hall effect in PtMn, with the highest value $\xi_{DL} = 0.24 \pm 0.03 = T_{\text{int}} \cdot \theta_{SH}^{\text{PtMn}}$ being obtained with a PtMn/Hf(0.25)/FeCoB multilayer, where T_{int} is the net interface spin transparency of that particular system. Assuming that the intrinsic spin Hall effect dominates in PtMn this result provides a lower bound for the spin Hall conductivity of PtMn $\sigma_{SH}^{\text{PtMn}} = (\xi_{DL} / T_{\text{int}}) \cdot \sigma_{\text{PtMn}} > 1.5 \times 10^5 (2e / \hbar) \Omega^{-1} \text{m}^{-1}$, since $T_{\text{int}} < 1$. This can be compared to the lower bound that has been established for Pt,

$\sigma_{SH}^{\text{Pt}} > 2.8 \times 10^5 (2e / \hbar) \Omega^{-1} \text{m}^{-1}$ from recent measurements of ξ_{DL} in the PMA Pt/Co system²⁷.

Refinements that yield a higher T_{int} for PtMn/FM interfaces will result in even higher ξ_{DL} . We conclude that PtMn in particular and likely other binary Pt compounds in general are very promising candidates as spin current sources and detectors in spintronics applications in both IPM and PMA systems provided that the interface can be engineered to have a high spin transparency.

Methods

Sample fabrication

All samples in this work were prepared by direct current (DC) sputtering (with RF magnetron sputtering for the MgO layer) in a deposition chamber with a base pressure $< 8 \times 10^{-8}$ Torr. The DC sputtering condition is 2mTorr Ar pressure, 30 watts power and low deposition rates (Ta: 0.0142 nm/s, PtMn: 0.0189 nm/s, FeCoB: 0.0064 nm/s, Co: 0.0066 nm/s). The PtMn alloy is deposited from a 2-inch planar Pt₅₀Mn₅₀ target. We utilized a Ta seeding layer as a template for smoothing the growth of the PtMn for all the standard stacking order samples. All samples have a Ta(1.5) top layer to provide an oxidized protection layer for the stack. We annealed the samples twice at 115 °C for 1 min as part of the photolithography process.

Acknowledgements

This research was supported by the Office of Naval Research, and by the NSF/MRSEC program (DMR-1120296) through the Cornell Center for Materials Research. We also acknowledge support from the NSF (Grant No. ECCS-1542081) through use of the Cornell Nanofabrication Facility/National Nanofabrication Infrastructure Network.

References

1. Miron, I. M. *et al.* Current-driven spin torque induced by the Rashba effect in a ferromagnetic metal layer. *Nat. Mater.* **9**, 230–4 (2010).
2. Miron, I. M. *et al.* Perpendicular switching of a single ferromagnetic layer induced by in-plane current injection. *Nature* **476**, 189–93 (2011).
3. Liu, L., Lee, O. J., Gudmundsen, T. J., Ralph, D. C. & Buhrman, R. A. Current-Induced Switching of Perpendicularly Magnetized Magnetic Layers Using Spin Torque from the Spin Hall Effect. *Phys. Rev. Lett.* **109**, 096602 (2012).
4. Liu, L. *et al.* Spin-torque switching with the giant spin Hall effect of tantalum. *Science* **336**, 555–8 (2012).
5. Chen, H., Niu, Q. & MacDonald, a. H. Anomalous Hall Effect Arising from Noncollinear Antiferromagnetism. *Phys. Rev. Lett.* **112**, 017205 (2014).
6. Mendes, J. B. S. *et al.* Large inverse spin Hall effect in the antiferromagnetic metal Ir₂₀Mn₈₀. *Phys. Rev. B* **89**, 140406 (2014).
7. Zhang, W. *et al.* Facet-dependent giant spin orbit torque in single crystalline antiferromagnetic Ir-Mn/ferromagnetic permalloy bilayers. *arXiv:1602.00670v1* (2016).
8. Zhang, W. *et al.* Spin Hall Effects in Metallic Antiferromagnets. *Phys. Rev. Lett.* **113**, 196602 (2014).
9. Fukami, S., Zhang, C., Duttagupta, S., Kurenkov, A. & Ohno, H. Magnetization switching by spin-orbit torque in an antiferromagnet / ferromagnet bilayer system. *Nat. Mater.* Advance online publication (2016). doi:10.1038/nmat4566
10. Zhang, W. *et al.* All-electrical manipulation of magnetization dynamics in a ferromagnet by antiferromagnets with anisotropic spin Hall effects. *Phys. Rev. B* **92**, 144405 (2015).
11. Tshitoyan, V. *et al.* Electrical manipulation of ferromagnetic NiFe by antiferromagnetic IrMn. *Phys. Rev. B* **92**, 214406 (2015).
12. Park, B. G. *et al.* A spin-valve-like magnetoresistance of an antiferromagnet-based tunnel junction. *Nat. Mater.* **10**, 347–351 (2011).

13. Barthem, V. M. T. S., Colin, C. V, Mayaffre, H., Julien, M.-H. & Givord, D. Revealing the properties of Mn₂Au for antiferromagnetic spintronics. *Nat. Commun.* **4**, 2892 (2013).
14. Marti, X. *et al.* Room-temperature antiferromagnetic memory resistor. *Nat Mater* **13**, 367–374 (2014).
15. Satoh, T., Iida, R., Higuchi, T., Fiebig, M. & Shimura, T. Writing and reading of an arbitrary optical polarization state in an antiferromagnet. *Nat. Photon.* **9**, 25 (2014).
16. Yang, S.-H., Ryu, K.-S. & Parkin, S. Domain-wall velocities of up to 750 m s⁻¹ driven by exchange-coupling torque in synthetic antiferromagnets. *Nat. Nanotechnol.* **10**, 221–226 (2015).
17. Jungwirth, T., Marti, X., Wadley, P. & Wunderlich, J. Antiferromagnetic spintronics. *Nat. Nanotechnol.* **11**, 231 (2016).
18. Rojas-Sánchez, J.-C. C. *et al.* Spin pumping and inverse spin hall effect in platinum: The essential role of spin-memory loss at metallic interfaces. *Phys. Rev. Lett.* **112**, 106602 (2014).
19. Meschel, S. V., Nash, P. & Chen, X. Q. The standard enthalpies of formation of binary intermetallic compounds of some late 4d and 5d transition metals by high temperature direct synthesis calorimetry. *J. Alloys Compd.* **492**, 105–115 (2010).
20. Liu, L., Moriyama, T., Ralph, D. C. & Buhrman, R. A. Spin-Torque Ferromagnetic Resonance Induced by the Spin Hall Effect. *Phys. Rev. Lett.* **106**, 036601 (2011).
21. Pi, U. H. *et al.* Tilting of the spin orientation induced by Rashba effect in ferromagnetic metal layer. *Appl. Phys. Lett.* **97**, 162507 (2010).
22. Kim, J. *et al.* Layer thickness dependence of the current-induced effective field vector in Ta|CoFeB|MgO. *Nat. Mater.* **12**, 240–5 (2013).
23. Nguyen, M.-H. *et al.* Enhancement of the anti-damping spin torque efficacy of platinum by interface modification. *Appl. Phys. Lett.* **106**, 222402 (2015).
24. Pai, C.-F., Ou, Y., Vilela-Leão, L. H., Ralph, D. C. & Buhrman, R. A. Dependence of the efficiency of spin Hall torque on the transparency of Pt/ferromagnetic layer interfaces. *Phys. Rev. B* **92**, 064426 (2015).
25. Pai, C.-F. *et al.* Enhancement of perpendicular magnetic anisotropy and transmission of spin-Hall-effect-induced spin currents by a Hf spacer layer in W/Hf/CoFeB/MgO layer structures. *Appl. Phys. Lett.* **104**, 082407 (2014).
26. Zhang, W., Han, W., Jiang, X., Yang, S.-H. & S. P. Parkin, S. Role of transparency of platinum–ferromagnet interfaces in determining the intrinsic magnitude of the spin Hall effect. *Nat. Phys.* **11**, 496 (2015).
27. Nguyen, M.-H., Ralph, D. C. & Buhrman, R. A. Spin torque study of the spin Hall conductivity and spin diffusion length in platinum thin films with varying resistivity. *Phys. Rev. Lett.* **116**, 126601 (2016).
28. Lee, O. J. *et al.* Central role of domain wall depinning for perpendicular magnetization switching driven by spin torque from the spin Hall effect. *Phys. Rev. B* **89**, 024418 (2014).
29. Liu, Y., Yuan, Z., Wesselink, R. J. H., Starikov, A. A. & Kelly, P. J. Interface Enhancement of Gilbert Damping from First Principles. *Phys. Rev. Lett.* **113**, 207202

(2014).

30. Tserkovnyak, Y., Brataas, A. & Bauer, G. Enhanced Gilbert Damping in Thin Ferromagnetic Films. *Phys. Rev. Lett.* **88**, 117601 (2002).
31. Tserkovnyak, Y., Brataas, A. & Bauer, G. Spin pumping and magnetization dynamics in metallic multilayers. *Phys. Rev. B* **66**, 224403 (2002).
32. Khvalkovskiy, A. V. *et al.* Matching domain-wall configuration and spin-orbit torques for efficient domain-wall motion. *Phys. Rev. B* **87**, 020402 (2013).

Figure 1

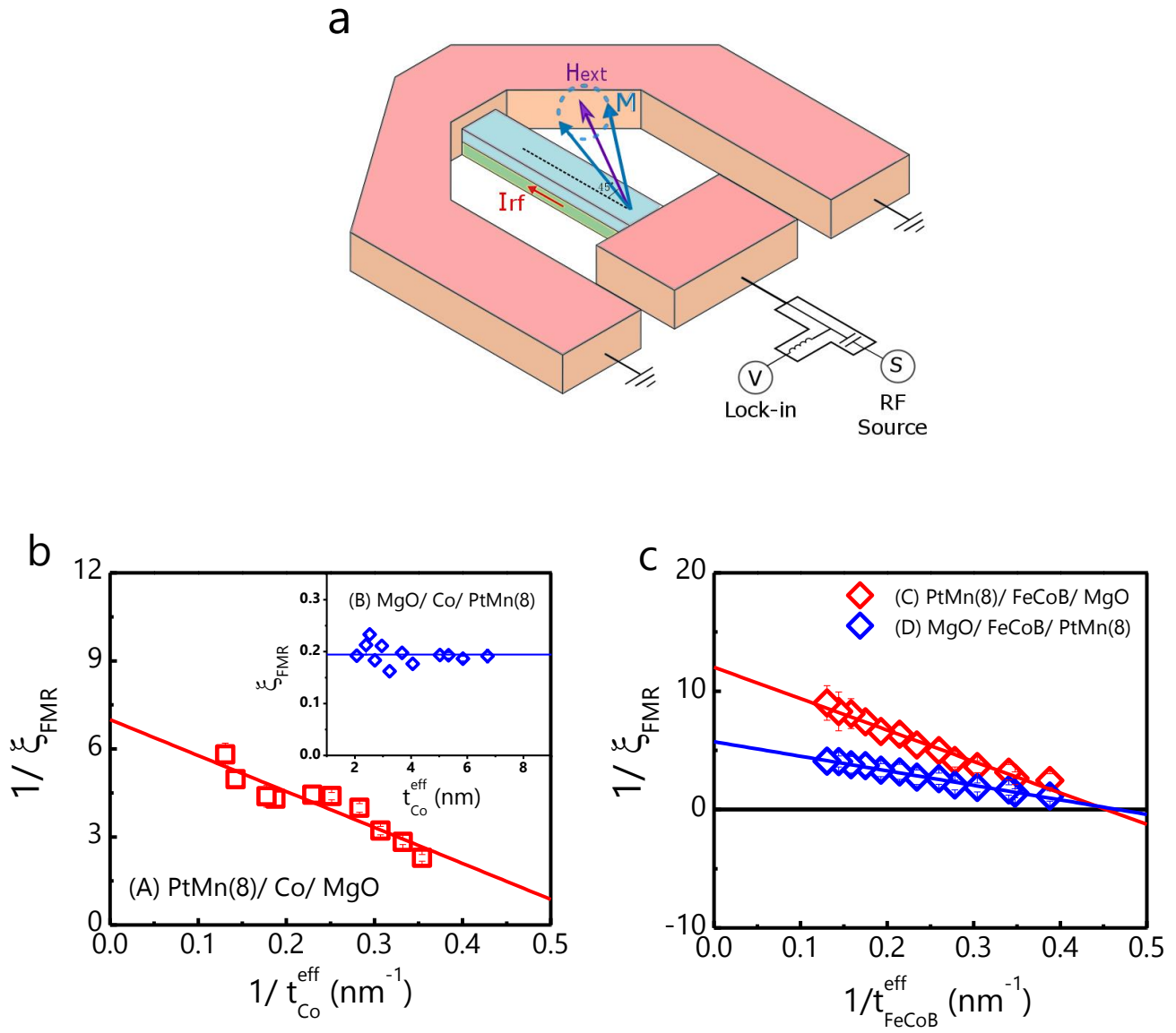


Figure 1: ST-FMR measurement on PtMn/Co and PtMn/FeCoB bilayer samples. **a.** Schematic of ST-FMR measurement. **b.** The inverse of the ST-FMR measured spin torque efficiency, $1/\xi_{FMR}$, as a function of the inverse of the effective thickness for the Co series (A) samples (red squares). Inset: ξ_{FMR} as a function of t_{Co}^{eff} for series (B) samples (blue squares). **c.** $1/\xi_{FMR}$ as a function of $1/t_{FeCoB}^{eff}$ for the series (C) (red squares) and series (D) (blue squares) samples.

Figure 2

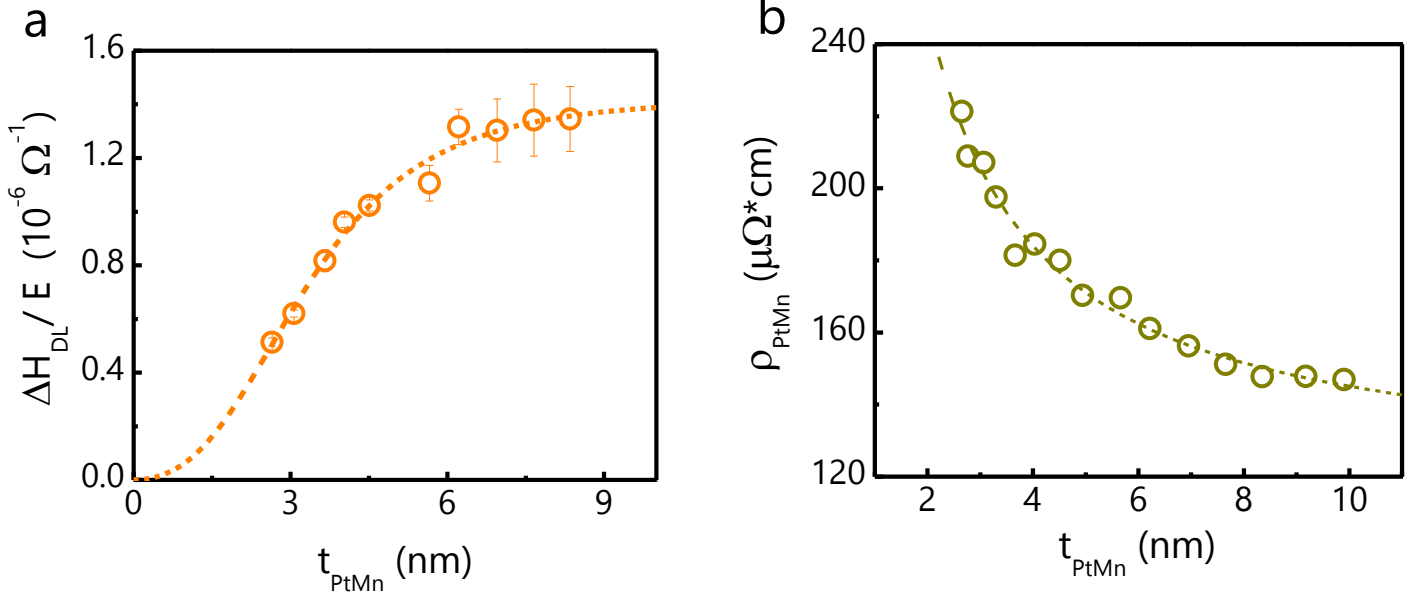


Figure 2: Spin diffusion length and resistivity measurement. **a**, Damping-like effective field per unit applied electric field for the series (G) samples as a function of PtMn thickness t_{PtMn} . **b**, Average resistivity of different thickness of PtMn as a function of t_{PtMn} . The dash line is a fit to the empirical function $\rho_0 + \rho_s / t_{PtMn}$ to the data, where ρ_0 and ρ_s are represent the bulk and interfacial scattering contributions to the resistivity.

Figure 3

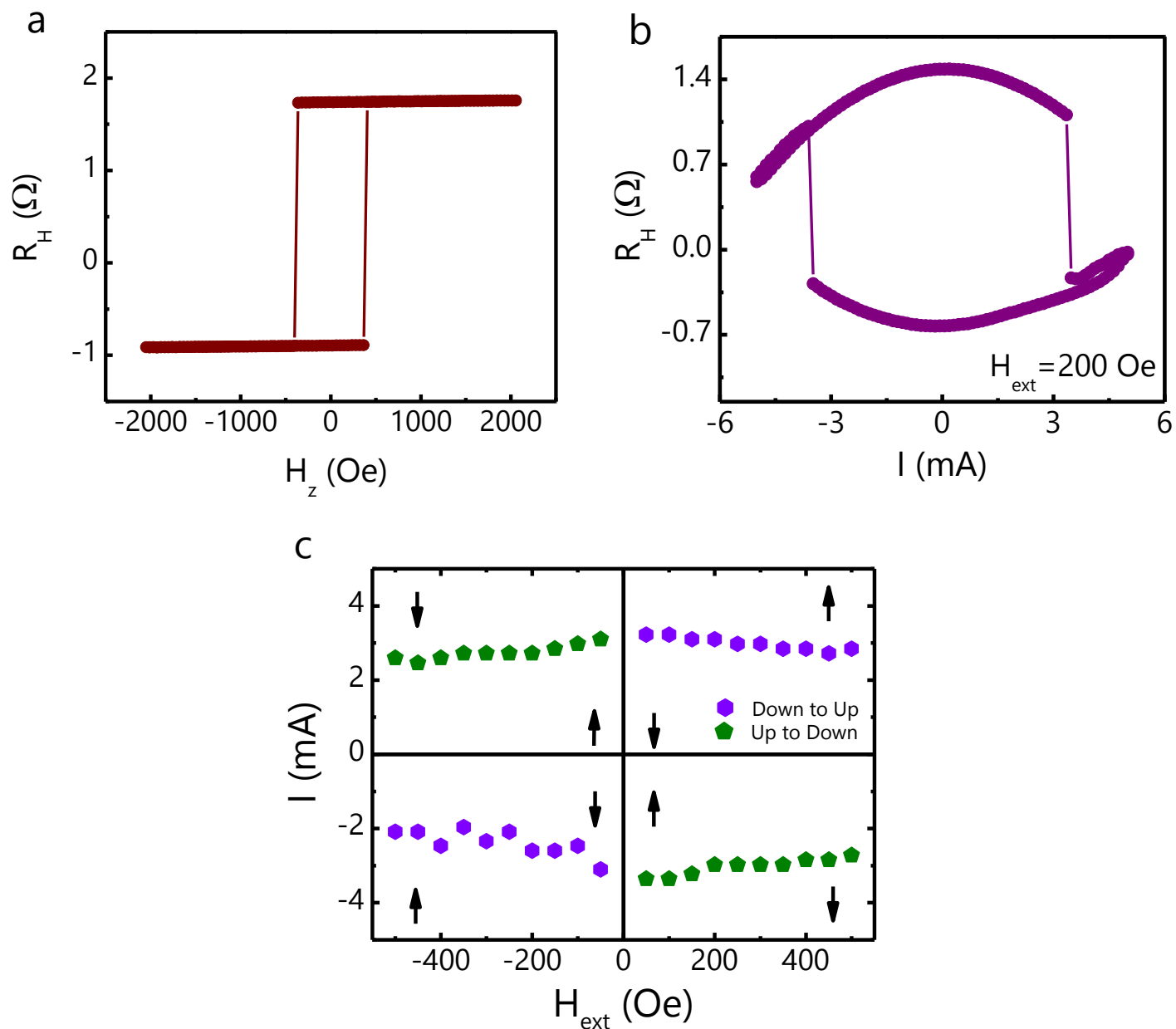


Figure 3: Field and current-induced switching. **a**, Magnetic field switching of a series (H) sample with the field perpendicular to the sample plane. **b**, Current-induced switching of same sample with an external magnetic field (200 Oe) applied in-plane along the current direction. **c**, Phase diagram of the current-induced switching.

Table I

Samples	Layer Structure	Stack order	ξ_{DL}	Anisotropy
(A)	Ta(1.5)/PtMn(8)/Co(t_{Co})/MgO(1.6)/Ta(1.5)	SO	0.16 ± 0.01	IPM
(B)	MgO(1.6)/Co(t_{Co})/PtMn(8)/MgO(1.6)/Ta(1.5)	RO	0.19 ± 0.02	IPM
(C)	Ta(1.5)/PtMn(8)/FeCoB(t_{FeCoB})/MgO(1.6)/Ta(1.5)	SO	0.096 ± 0.03	IPM
(D)	MgO(1.6)/FeCoB(t_{FeCoB})/PtMn(8)/MgO(1.6)/Ta(1.5)	RO	0.174 ± 0.04	IPM
(E)	Ta(1.5)/PtMn(8)/FeCoB(0.8)/MgO(1.6)/Ta(1.5)	SO	0.11 ± 0.02	PMA
(F)	Ta(1.5)/PtMn(8)/Hf(0.25)/FeCoB(0.8)/MgO(1.6)/Ta(1.5)	SO	0.24 ± 0.03	PMA

Table I. A summary of the parameters of the different samples of samples in this study: Here || represents the Si/SiO₂ substrate, SO(RO) means “standard order” (“reverse order”) of stack growth, ξ_{DL} is the anti-damping spin torque efficiency of each samples, and IPM (PMA) means the sample is in-plane (out-of-plane) magnetized.

Supplementary Material

Strong Spin Hall Effect in the Antiferromagnet PtMn

Yongxi Ou¹, Shengjie Shi¹, D. C. Ralph^{1,2}, and R. A. Buhrman^{1,*}

¹Cornell University, Ithaca, New York 14853, USA

²Kavli Institute at Cornell, Ithaca, New York 14853, USA

Contents

S1. ST-FMR formula for samples with a non-negligible field-like component of spin torque

S2. Determination of PMA in Ta/PtMn(8)/FeCoB(t_{FeCoB})/MgO samples

S3. Measurement of the spin diffusion length in PtMn

S4. X-ray diffraction results

S5. Damping measurement and spin mixing conductance calculation

S1. ST-FMR formula for systems with a non-negligible field-like term

We use the definition utilized in Ref. [1, 2]:

$$\xi_{FMR} = \frac{S}{A} \left(\frac{e}{\hbar} \right) 4\pi M_s t_{FM}^{\text{eff}} d_{NM} \sqrt{1 + (4\pi M_{\text{eff}} / H_0)} \quad (1)$$

where e , \hbar , $4\pi M_s$, t_{FM}^{eff} , d_{NM} , H_0 represent the electron charge, the Planck constant, the magnetization, the effective thickness of FM layer, the thickness of NM layer, the effective demagnetization field of FM layer, and the ferromagnetic resonance field, respectively. S is the symmetric component of the ST-FMR resonance about the resonant field and A is the antisymmetric component. For a HM/FM bilayer system in which there is a damping-like torque τ_{DL} acting on the FM, but no field-like torque τ_{FL} , ξ_{FMR} is simply equal to the anti-damping spin torque efficiency ξ_{DL} . However if the field-like spin torque efficiency ξ_{FL} is not negligible, one can express $S(A)$ as:

$$S = \frac{\hbar}{2e} \frac{\xi_{DL} J_e^{\text{rf}}}{4\pi M_s t_{FM}^{\text{eff}}} \quad (2)$$

$$A = (H_T + H_{Oe}) \sqrt{1 + (4\pi M_{\text{eff}} / H_0)} = \left(\frac{\hbar}{2e} \frac{\xi_{FL} J_e^{\text{rf}}}{4\pi M_s t_{FM}^{\text{eff}}} + \frac{J_e^{\text{rf}} d_{NM}}{2} \right) \sqrt{1 + (4\pi M_{\text{eff}} / H_0)} \quad (3)$$

where J_e^{rf} , $H_T \propto \tau_{DL}$, H_{Oe} are the electric current density, field-like effective field and the Oersted field, respectively. Combining Eqs. (1)-(3), we have:

$$\frac{1}{\xi_{FMR}} = \frac{1}{\xi_{DL}} \left(1 + \frac{\hbar}{e} \frac{\xi_{FL}}{4\pi M_s t_{FM}^{\text{eff}} d_{NM}} \right) \quad (4)$$

As long as ξ_{FL} is independent of FM thickness, then $1/\xi_{FMR}$ will be a linear function of $1/t_{FM}^{eff}$, from which the intercept and slope allow a determination of ξ_{DL} and ξ_{FL} . We use Eq. (4) to fit the ST-FMR data for IPM series (A)-(D) samples in the main text.

S2. Determination of PMA in Ta/PtMn(8)/FeCoB(t_{FeCoB})/MgO samples

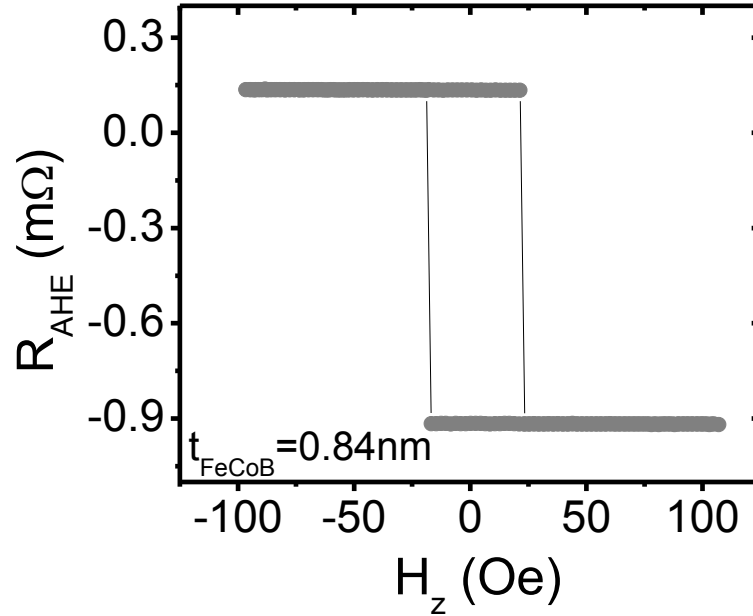


Figure S2: Anomalous hall measurement. Anomalous Hall resistance of sample Ta(1.5)/PtMn(8)/FeCoB(t_{FeCoB})/MgO(1.6)/Ta(1.5) when t_{FeCoB} is equal to 0.84 nm.

We determined the thickness range for FeCoB that yields PMA for the multilayer Ta(1.5)/PtMn(8)/FeCoB(t_{FeCoB})/MgO(1.6)/Ta(1.5) by performing anomalous Hall resistance measurements under an external magnetic field applied perpendicular to the film plane. A typical sample is shown in Fig. S2. We found the PMA thickness range for this sample to be $0.6 \text{ nm} < t_{\text{FeCoB}} < 1.0 \text{ nm}$, with the strongest PMA occurring when $t_{\text{FeCoB}} \sim 0.77 \text{ nm}$.

S3. Spin diffusion length measurement of PtMn

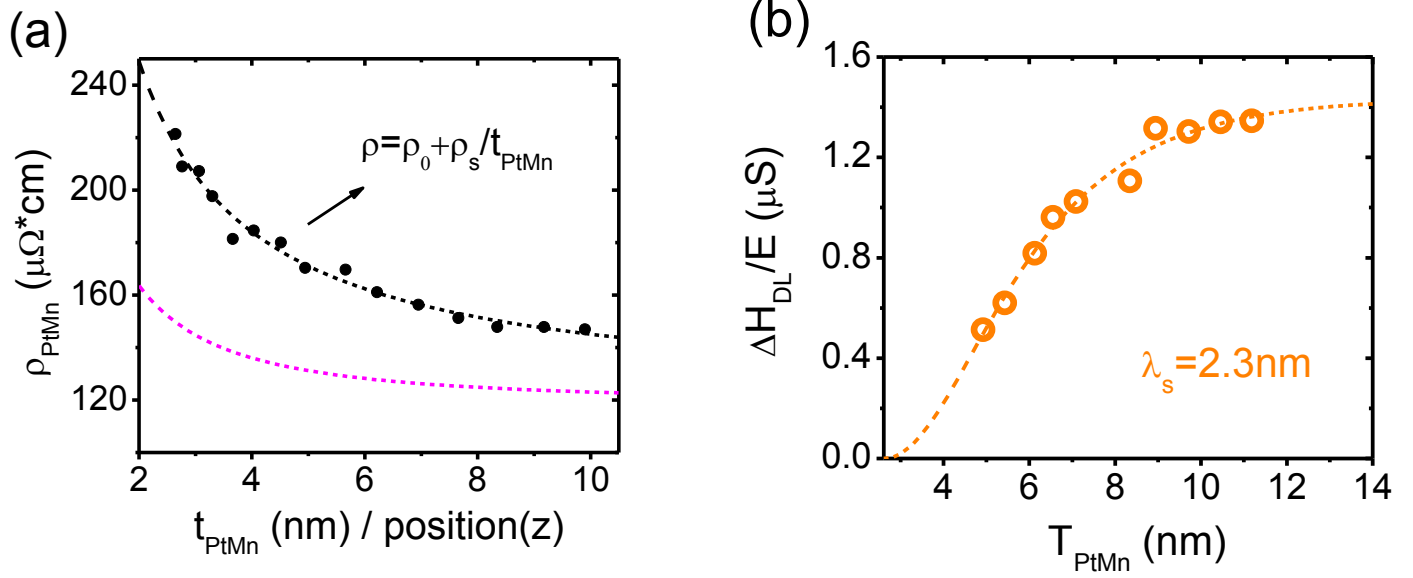


Figure S3: Resistivity and spin diffusion length measurement. **a**, The measured average resistivity and local resistivity of PtMn in series (B) samples. The black dashed line is a fit to the average resistivity while purple dashed line represents the calculated local resistivity. **b**, Damping-like effective spin-torque field per unit applied electric field as a function of the effective thickness of PtMn. The dash line represents a fit using Eq. (9).

In a diffusive model for spin transport within a PtMn(t_{PtMn})/Hf/FeCoB trilayer, the damping-like spin torque efficiency should depend on the PtMn thickness t_{PtMn} as²⁴:

$$\xi_{DL} = \theta_{SH} (1 - \text{sech}(\frac{t_{\text{PtMn}}}{\lambda_{\text{PtMn}}})) \frac{G^*}{G^* + G_{\text{PtMn}} \tanh(t_{\text{PtMn}} / \lambda_{\text{PtMn}})} \text{sech}(\frac{t_{\text{Hf}}}{\lambda_{\text{Hf}}}) \frac{2 \text{Re}(G^{\uparrow\downarrow})}{2 \text{Re}(G^{\uparrow\downarrow}) + G_{\text{Hf}}} \quad (5)$$

Here t_{Hf} , λ_{Hf} , G_{Hf} are the thickness, the spin diffusion length and spin conductance of Hf (with

$G_{\text{Hf}} = 1/(\rho_{\text{Hf}} \lambda_{\text{Hf}})$), and

$$G^* = G_{\text{Hf}} \coth(\frac{t_{\text{Hf}}}{\lambda_{\text{Hf}}}) \frac{G_{\text{Hf}} \tanh(\frac{t_{\text{Hf}}}{\lambda_{\text{Hf}}}) + 2 \text{Re}(G^{\uparrow\downarrow})}{G_{\text{Hf}} \coth(\frac{t_{\text{Hf}}}{\lambda_{\text{Hf}}}) + 2 \text{Re}(G^{\uparrow\downarrow})} \quad (6)$$

We define the anti-damping spin torque effective field DH_{DL} such that³²:

$$\xi_{DL} = \left(\frac{2e}{\hbar} \right) 4\pi M_s t_{FM}^{\text{eff}} \left(\frac{\Delta H_{DL}}{J_e} \right) \quad (7)$$

Combining Eqs. (5) and (7) gives:

$$\frac{\Delta H_{DL}}{E} = \frac{\sigma_{SH}}{4\pi M_s t_{FM}^{\text{eff}}} \frac{G_A}{G_{\text{PtMn}} \tanh(t_{\text{PtMn}} / \lambda_{\text{PtMn}}) + G_B} (1 - \text{sech}(t_{\text{PtMn}} / \lambda_{\text{PtMn}})) \quad (8)$$

where G_A (G_B) is a parameter depending on the Hf spacer and spin mixing conductance at Hf/FeCoB. This is Eq. (1) in the main text.

We used Eq. (8) to fit the data in Fig. 2a (main text) to obtain an effective spin diffusion length of PtMn = 2.1 nm. However, Eq. (8) assumes that the spin diffusion length and the spin Hall ratio in the PtMn layer are both constant, independent of t_{PtMn} . This is not necessarily the

case if the PtMn resistivity ρ_{PtMn} varies with film thickness over the range that we are employing. In this case if the spin relaxation in PtMn is dominated by the Elliot-Yafet scattering mechanism where $\rho_{\text{PtMn}} \times \lambda_s^{\text{PtMn}}$ is the constant quantity, λ_s^{PtMn} will vary with t_{PtMn} . In addition, if the spin Hall effect in PtMn is dominant by the intrinsic process, rather than by extrinsic skew-scattering, the spin Hall ratio is not constant but varies linearly with resistivity, $\theta_{SH}^{\text{PtMn}} = (\hbar / 2e) \rho_{\text{PtMn}} \times \sigma_{SH}^{\text{PtMn}}$, where $\sigma_{SH}^{\text{PtMn}}$ is the spin Hall conductivity and is expected to be constant when the resistivity is altered by a change in the elastic and quasi-elastic scattering rates within the material. The resistivity of our PtMn thin films as averaged over the thickness of each film is shown in Fig. 2b (main text) as a function of t_{PtMn} , and there is clearly a substantial variation from 2 nm to 10 nm. In a recent report on the thickness dependent spin Hall properties of Pt thin films, our group has proposed a “rescaling” method for dealing with this effect in the case of Elliot-Yafet spin scattering and the intrinsic spin Hall effect regime²⁷. Here we use a similar treatment to our PtMn data. First we measured the resistivity of PtMn layer in sample (F) Ta(1)/PtMn(t_{PtMn})/Hf(0.8)/FeCoB(0.7)/MgO by comparing its resistance to a control sample without PtMn layer: Ta(1)/ Hf(0.8)/FeCoB(0.7)/MgO. The resistance and thus resistivity of PtMn layer can be determined from the parallel resistance model. The result is shown in Fig. 3(a) in the main text and in Fig. S4(a) with black dots. We used the form $\rho(t_{\text{PtMn}}) = \rho_0 + \rho_s / t_{\text{PtMn}}$ to fit the data, in which ρ_0 and ρ_s represent the bulk and interfacial scattering contribution to the average resistivity $\rho(t_{\text{PtMn}})$ for a certain thickness of PtMn. The fit (black dashed line) in Fig. S3(a) gives $\rho_0 = 119 \mu\Omega\text{cm}$ and $\rho_s = 2.6 \times 10^{-5} \mu\Omega\text{cm}^2$. Then by considering that a certain thickness of PtMn layer consists of slices of PtMn thin films with varying resistivity, we calculated the “local resistivity” $\rho(z)$ of PtMn as $\rho(z) = (\rho_0 + \rho_s / z)^2 / (\rho_0 + 2\rho_s / z)$, shown as

the purple dashed line in Fig. S3(a). Based on $\rho(z)$, we can transform the thickness of PtMn t_{PtMn} into an effective thickness T_{PtMn} with the same spin diffusion length λ_0 corresponding to the bulk value of resistivity ρ_0 , and Eq. (8) becomes:

$$\frac{\Delta H_{DL}}{E} = \frac{\sigma_{SH}}{4\pi M_s t_{FM}^{\text{eff}} G_{\text{PtMn}}} \frac{G_A}{\tanh((T_{\text{PtMn}} - T_0) / \lambda_0) + G_B} (1 - \text{sech}((T_{\text{PtMn}} - T_0) / \lambda_0)) \quad (9)$$

The fit using Eq. (9) gives $\lambda_0 = 2.3$ nm, shown in Fig. S3(b).

S4. X-ray diffraction measurement

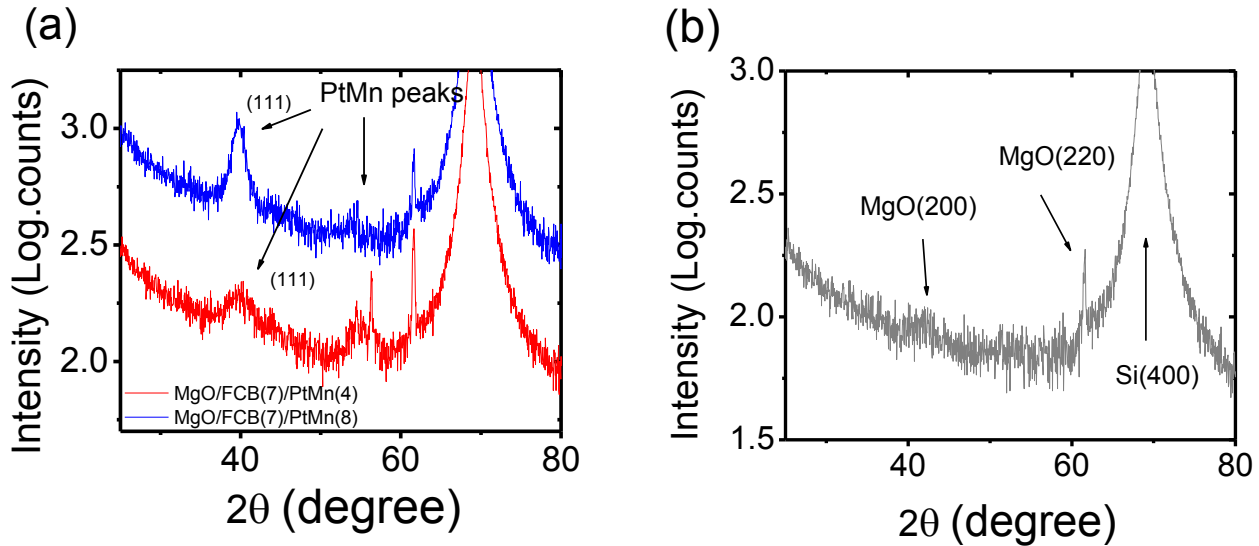


Figure S4: X-ray diffraction measurement. XRD pattern for **a**, sample MgO(1.6)/FeCoB(7)/PtMn(4)/MgO(1.6)/Ta(1.5) (red) and MgO(1.6)/FeCoB(7)/PtMn(8)/MgO(1.6)/Ta(1.5) (blue), and **b**, a reference sample MgO(1.6)/FeCoB(7)/MgO(1.6)/Ta(1.5). The signals in (a) have been shifted in the y-direction to allow for comparison.

We obtained x-ray diffraction spectra from samples MgO(1.6)/FeCoB(7)/PtMn(4,8)/MgO(1.6)/Ta(1.5), as shown in Fig. S4 (a). The main PtMn (111) peak is observed at around $2\theta \sim 40^\circ$. With the thinner PtMn layer (4 nm), the peak is lower and broader in comparison to that of the thicker PtMn (8 nm) layer. This is consistent with the thicker PtMn sample having somewhat larger crystalline domains. There is also a secondary

peak centered at $2\theta \sim 55^\circ$, which we have not identified but does appear to arise from the PtMn.

Fig. S4(b) shows the x-ray diffraction measured for a reference sample

MgO(1.6)/FeCoB(7)/MgO(1.6)/Ta(1.5), which has the same stacking order and structure as sample (D) without the PtMn layer.

S5. Damping measurement and spin mixing conductance calculation

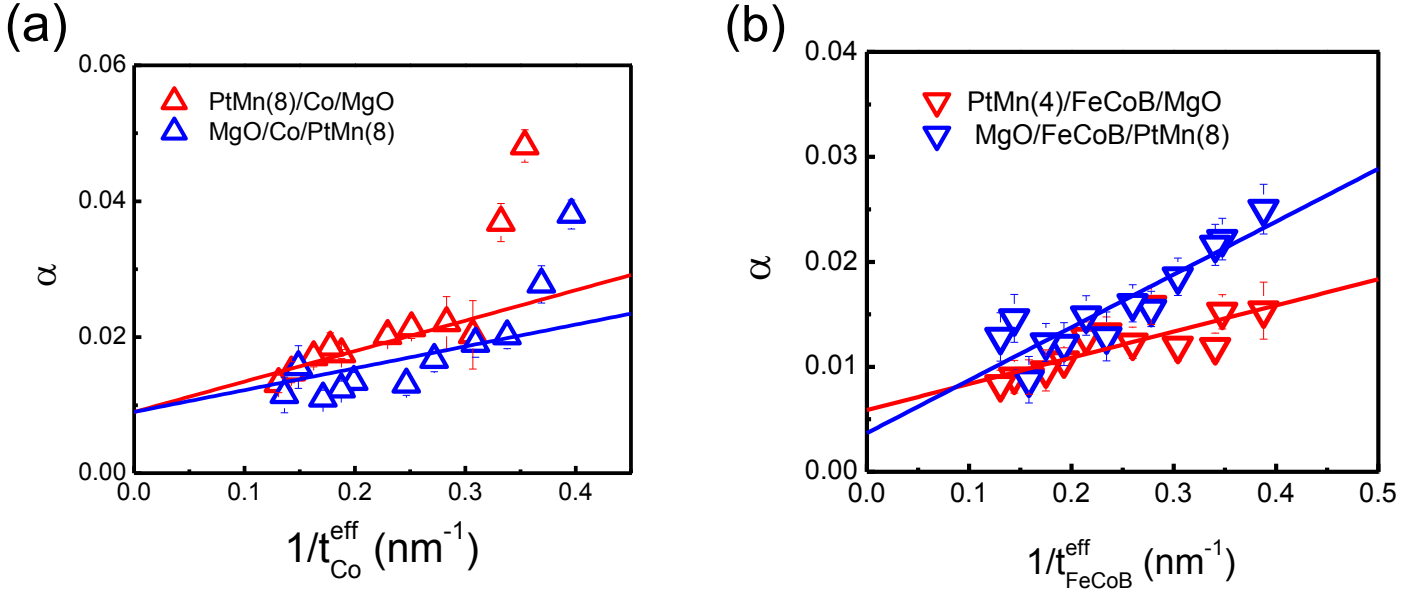


Figure S5: Damping measurements: **a,b**, Enhanced damping as a function of the inverse of the effective thickness for Co samples SO series (A) (red triangles) and RO series (B) (blue triangles), and FeCoB samples SO series (C) (red triangles) and RO series (D) (blue triangles).

According to the conventional spin pumping theory^{30,31}, by measuring the enhancement of the damping constant $\Delta\alpha$ as a function of the FM layer thickness, as shown in Fig. 5, and provided that there are no other interfacial contributions to the damping, such as SML or a magnetic “dead layer,” one can determine the interfacial spin-mixing conductance:

$$\Delta\alpha = \alpha - \alpha_0 = \frac{\gamma\hbar}{4\pi M_s t_{FM}^{\text{eff}}} g_{\text{eff}}^{\uparrow\downarrow} = \frac{\gamma\hbar^2}{8\pi^2 e^2 M_s t_{FM}^{\text{eff}}} G_{\text{eff}}^{\uparrow\downarrow} \quad (10)$$

Here α_0 and $\gamma = 1.76 \times 10^{11} \text{ s}^{-1} \text{ T}^{-1}$ represent the intrinsic damping constant and the gyromagnetic ratio of the FM layer. $g_{\text{eff}}^{\uparrow\downarrow} (G_{\text{eff}}^{\uparrow\downarrow})$ is the so-called interfacial spin-mixing conductance, which is related to the spin current transparency at the PtMn/FM interface^{24,26} (with $G_{\text{eff}}^{\uparrow\downarrow} = (e^2 / h) g_{\text{eff}}^{\uparrow\downarrow}$). However, if additional spin attenuation occurs in the interfaces of the FM layer, that would contribute to $g_{\text{eff}}^{\uparrow\downarrow}$, making it larger than the value given only by spin pumping²⁴, leading to an over-estimate of the true interfacial spin-mixing conductance. Fitting the data in Fig. S5 gives the apparent $g_{\text{eff}}^{\uparrow\downarrow} (G_{\text{eff}}^{\uparrow\downarrow})$ as summarized in the following table for samples (A)-(D):

Sample	Apparent $g_{\text{eff}}^{\uparrow\downarrow} \text{ (nm}^{-2}\text{)}$	Apparent $G_{\text{eff}}^{\uparrow\downarrow} = (e^2 / h) g_{\text{eff}}^{\uparrow\downarrow} \text{ (} 10^{15} \Omega^{-1} \text{m}^{-2}\text{)}$
A	40.8	1.58
B	33.4	1.29
C	18.8	0.72
D	39.4	1.53

The bare spin mixing conductance $G^{\uparrow\downarrow}$ of the interface can be expressed as²⁴:

$$G^{\uparrow\downarrow} = \frac{G_{\text{eff}}^{\uparrow\downarrow}}{1 - 2 \frac{G_{\text{eff}}^{\uparrow\downarrow}}{G_{\text{PtMn}}}} \quad (11)$$

If we use the result $G_{\text{PtMn}} = 1 / (\rho_{\text{PtMn}} \lambda_{\text{PtMn}}) = 0.37 \times 10^{15} \Omega^{-1} \text{m}^{-2}$ (from section S3 above), one can see that $G^{\uparrow\downarrow}$ will have to be negative for all four samples, which is unphysical. This is also the case if we use the measured values $\rho_{\text{PtMn}} = 164 \mu\Omega\text{cm}$ and $\lambda_{\text{PtMn}} = 0.5 \text{ nm}$ from previous PtMn

research⁸. This suggests again that the measured $g_{\text{eff}}^{\uparrow\downarrow}$ cannot be explained by the conventional bilayer spin pumping model and extra interfacial spin attenuation factors (not related to injection of spin current into the HM) have to be included to account for the large measured values of $g_{\text{eff}}^{\uparrow\downarrow}$.

Reference:

1. Liu, L., Moriyama, T., Ralph, D. C. & Buhrman, R. A. Spin-Torque Ferromagnetic Resonance Induced by the Spin Hall Effect. *Phys. Rev. Lett.* **106**, 036601 (2011).
2. Pai, C.-F., Ou, Y., Vilela-Leão, L. H., Ralph, D. C. & Buhrman, R. A. Dependence of the efficiency of spin Hall torque on the transparency of Pt/ferromagnetic layer interfaces. *Phys. Rev. B* **92**, 064426 (2015).
3. Khvalkovskiy, A. V. *et al.* Matching domain-wall configuration and spin-orbit torques for efficient domain-wall motion. *Phys. Rev. B* **87**, 020402 (2013).
4. Nguyen, M.-H., Ralph, D. C. & Buhrman, R. A. Spin torque study of the spin Hall conductivity and spin diffusion length in platinum thin films with varying resistivity. *Phys. Rev. Lett.* **116**, 126601 (2016).
5. Tserkovnyak, Y., Brataas, A. & Bauer, G. Enhanced Gilbert Damping in Thin Ferromagnetic Films. *Phys. Rev. Lett.* **88**, 117601 (2002).
6. Tserkovnyak, Y., Brataas, A. & Bauer, G. Spin pumping and magnetization dynamics in metallic multilayers. *Phys. Rev. B* **66**, 224403 (2002).
7. Zhang, W., Han, W., Jiang, X., Yang, S.-H. & S. P. Parkin, S. Role of transparency of platinum–ferromagnet interfaces in determining the intrinsic magnitude of the spin Hall effect. *Nat. Phys.* **11**, 496 (2015).
8. Zhang, W. *et al.* Spin Hall Effects in Metallic Antiferromagnets. *Phys. Rev. Lett.* **113**, 196602 (2014).